Reviewed Preprint
v1 • July 20, 2026
Not revised

For correspondence:
kurumizaka@iqb.u-tokyo.ac.jp

Competing interests: No competing interests declared

Funding: See page 13

Reviewing editor: Volker Dötsch, Goethe University Frankfurt, Germany

Structural basis for site-specific histone H3 acetylation-dependent regulation of RNAPII transcription through nucleosomes

Takumi Oishi[1,2], Suguru Hatazawa[1], Tomoya Kujirai[1,4], Sae Suzuki[3], Koki Nakatsu[3], Gosuke Hayashi[3], Junko Kato[1], Yuki Kobayashi[1], Mitsuo Ogasawara[1], Haruhiko Ehara[4], Shun-ichi Sekine[4], Yoshimasa Takizawa[1,5], Hitoshi Kurumizaka[1,2,4,6]

[1]Laboratory of Chromatin Structure and Function, Institute for Quantitative Biosciences, The University of Tokyo, Tokyo, Japan • [2]Department of Biological Sciences, Graduate School of Science, The University of Tokyo, Tokyo, Japan • [3]Department of Biomolecular Engineering, Graduate School of Engineering, Nagoya University, Nagoya, Japan • [4]RIKEN Center for Integrative Medical Sciences, Yokohama, Japan • [5]Department of Computational Biology and Medical Sciences, Graduate School of Frontier Sciences, The University of Tokyo, Tokyo, Japan • [6]Division of Chromatin Structure and Function, Department of Multidisciplinary Life Science, Medical Institute of Bioregulation, Kyushu University, Fukuoka, Japan

eLife Assessment

This manuscript describes a **valuable** study of the mechanism by which acetylation on the histone H3 core domain regulates RNA polymerase II transcription passing through nucleosomes. The authors provide **convincing** evidence that acetylation influences transcription in a context-specific fashion. Some questions relating to the static nucleosome structures and the polymerase passage remain, but this manuscript will be of considerable interest to researchers in the chromatin and transcription fields.

https://doi.org/10.7554/eLife.111802.1.sa3

Abstract

Acetylation of histone H3 regulates chromatin dynamics and transcription, but how specific acetylation sites affect RNA polymerase II (RNAPII) transcription through nucleosomes remains unclear. Here, we found that H3 acetylation at Lys56 and Lys122 markedly enhances RNAPII transcription through nucleosomes, whereas acetylation at Lys64 has little effect. To elucidate the structural basis for these functional differences, we determined cryo-electron microscopy (cryo-EM) structures of nucleosomes bearing site-specific acetylation at H3K56, H3K64, or H3K122. The cryo-EM structures revealed that H3K56ac and H3K122ac locally weaken histone-DNA interactions at the DNA entry/exit region and near the dyad, respectively, while H3K64ac induces no detectable structural changes. These structural differences correlate with the observed transcriptional outcomes, indicating that acetylation at H3K56 and H3K122, but not H3K64, alleviates the nucleosomal barrier to RNAPII progression. Our findings provide direct structural evidence that specific acetylations within the histone fold domain of H3 finetune nucleosome dynamics to facilitate RNAPII transcription.

Introduction

Chromatin plays a central role in regulating access to genomic DNA during fundamental cellular processes such as transcription, replication, and DNA repair (1). The basic structural unit of chromatin is the nucleosome, which comprises approximately 147 base pairs of DNA wrapped

around a histone octamer containing two copies each of histones H2A, H2B, H3, and H4 (2, 3). The positions in nucleosomal DNA are designated as superhelical locations (SHLs) (4). By defining the center of the nucleosomal DNA as SHL(0), which corresponds to the dyad axis of the nucleosome, DNA positions at roughly every 10 base pairs are assigned as SHL(±1) to SHL(±7) (2, 4). The dynamic nature of nucleosomes is tightly regulated by post-translational modifications (PTMs) of histones, which can modulate histone-DNA and histone-protein interactions to influence chromatin accessibility (5–7). Among these modifications, the acetylation of lysine residues on histone H3 has long been associated with transcriptional activation, by promoting an open chromatin conformation conducive to gene expression (8, 9).

While histone acetylation is generally thought to weaken histone-DNA contacts by neutralizing the positive charge of lysine side chains (10), how individual acetylation sites contribute to chromatin dynamics and transcriptional regulation remains poorly understood. In particular, the lysine residues within the histone H3 core domain, such as Lys56 (K56), Lys64 (K64), and Lys122 (K122), are positioned at key DNA-histone interfaces and have been implicated in modulating nucleosome stability (6, 11–13). H3K56 acetylation occurs at the DNA entry/exit region and has been linked to nucleosome assembly, disassembly, and replication-coupled chromatin remodeling (14–17). The acetylation of H3K122, located near the nucleosomal dyad, has been reported to directly destabilize histone-DNA contacts, promoting nucleosome sliding and transcriptional activation (18–22). Similarly, the acetylation of H3K64, positioned within the nucleosome core, facilitates nucleosome instability and promotes chromatin accessibility, correlating with transcriptionally active regions (13, 23). However, the mechanisms by which these modifications alter the nucleosome architecture to facilitate RNA polymerase II (RNAPII) transcription remain elusive.

In the present study, we found that the acetylation of histone H3 at Lys56 and Lys122 markedly enhances RNA polymerase II (RNAPII) transcription through nucleosomes, whereas the acetylation at Lys64 has little effect. To elucidate the structural basis for these functional differences, we determined cryo-electron microscopy (cryo-EM) structures of nucleosomes containing site-specifically acetylated H3 at Lys56, Lys64, or Lys122. The structures revealed that H3K56ac and H3K122ac locally weaken histone-DNA interactions at the DNA entry/exit region and near the dyad, respectively, whereas H3K64ac causes no detectable changes. These distinct structural consequences of acetylation within the histone fold domain of H3 provide a mechanistic framework for understanding how specific lysine modifications fine-tune nucleosome dynamics to facilitate RNAPII transcription.

Results

Preparation of site-specifically acetylated nucleosomes for RNAPII transcription

To investigate how specific acetylation sites within the histone fold domain of histone H3 influence nucleosome structure and transcription, we prepared human histone H3 bearing the site-specific acetylation of Lys56, Lys64, or Lys122 (H3K56ac, H3K64ac, and H3K122ac) by chemical synthesis (Figure 1A and B, Supplementary Figure 1A). Each acetylated histone H3 was obtained through native chemical ligation with synthetic acetylated and non-acetylated peptides. In this method, we employed the H3.2 C110A mutant, in which the Cys110 residue of H3.2 was replaced by Ala, because the Cys residue is converted into the Ala residue during the desulfurization process after peptide ligation. We prepared histone octamers containing recombinant histones H2A, H2B, H4, and the synthesized H3.2 containing H3K56ac, H3K64ac, or H3K122ac. Nucleosomes containing H3K56ac, H3K64ac, and H3K122ac were then reconstituted using a 198 base-pair (bp) DNA fragment consisting of a modified Widom 601 sequence containing a 9-base mismatched region in a linker DNA (24) (Supplementary Figure 1B and C). RNAPII associates with the 9-base mismatched region and initiates transcription by the addition of nucleotide triphosphates and a primer RNA. We then performed in vitro nucleosome transcription assays using purified Komagataella phaffii RNAPII and its essential elongation factor, TFIIS (Figure 1C).

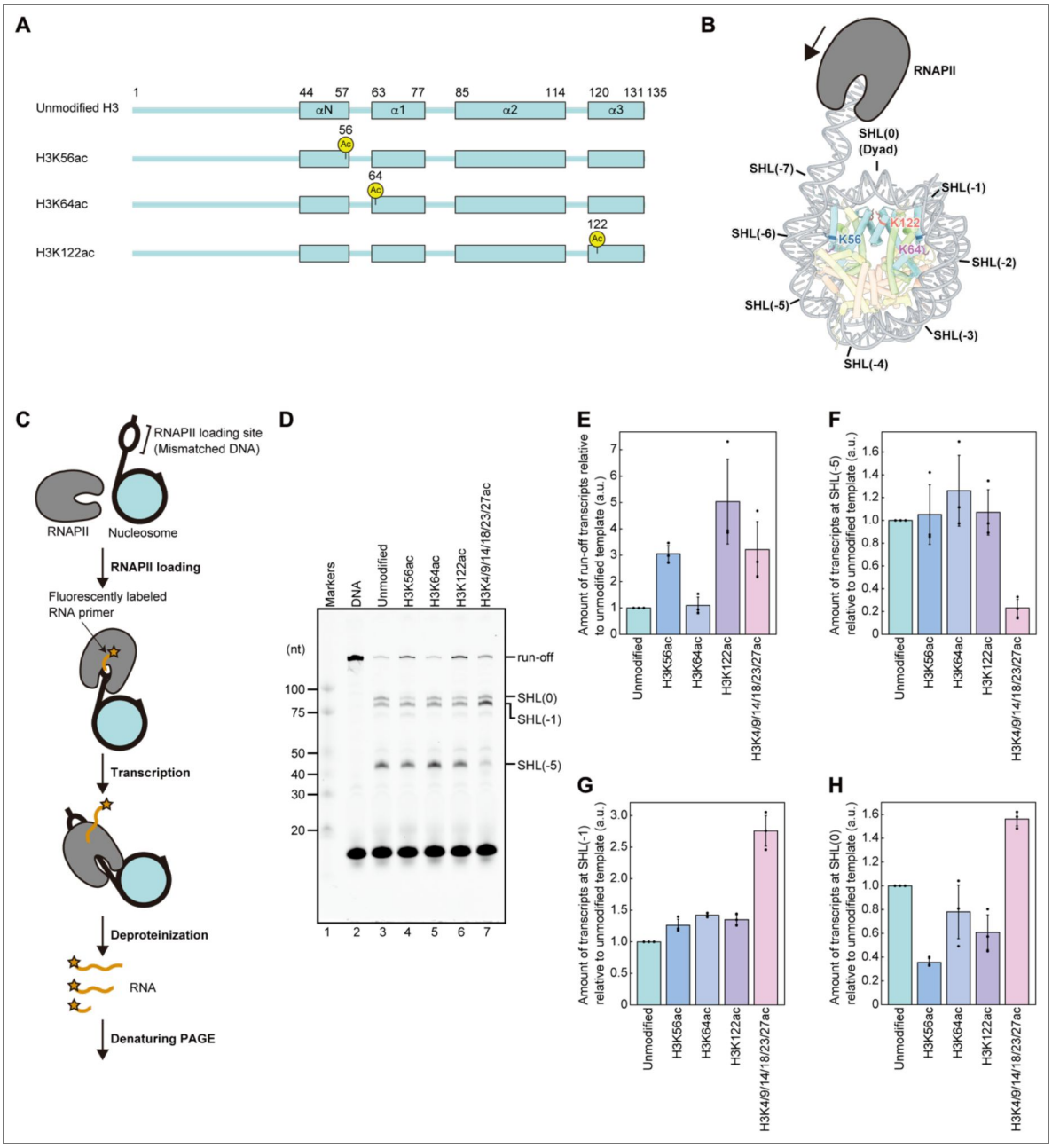

Figure 1. Acetylation at Lys56 or Lys122 of H3 decreases transcription barrier at SHL(0) and facilitates RNAPII progression.

(A) Secondary structure of histone H3, showing the acetylated residues (yellow). (B) SHLs, transcription direction, and Lys56, Lys64, and Lys122 are shown on the nucleosome structure (PDB ID: 7K61). Histones H2A, H2B, H3, H4, and DNA are colored pale yellow, pale red, pale blue, pale green, and gray, respectively. Lys56, Lys64, and Lys122 are shown in blue, purple, and orange, respectively. (C) Schematic representation of the transcription assay. (D) Transcription assays using free DNA, and unmodified, H3K56ac, H3K64ac, H3K122ac, and H3K4/9/14/18/23/27ac nucleosome templates. RNA transcripts were analyzed by denaturing PAGE and detected by DY647 fluorescence. (E-H) Quantification of transcripts corresponding to (E) run-off, (F) SHL(-5), (G) SHL(-1), and (H) SHL(0) positions. Amounts of transcripts were normalized to those of the unmodified nucleosome template. Bar graphs show the means of three independent experiments, and dots indicate the individual values. Error bars represent the standard deviation.

Site-specific acetylations of the histone fold domain of H3 differently modulate nucleosome transcription by RNAPII

When RNAPII transcribed through the unmodified nucleosome, an RNA transcript of approximately 40 nucleotides, which corresponds to the RNAPII pausing at the SHL(-5), was predominantly accumulated (Figure 1D, lane 3, Supplementary Figure 2). In addition, RNA products around 75-80 nucleotides, which correspond to the RNAPII pausing at the SHL(-1) and SHL(0) positions, were also detected (Figure 1D, lane 3). Notably, run-off transcripts were barely detectable in the unmodified nucleosome template (Figure 1D, lane 3). These results are consistent with the previous studies (24) and indicate that the nucleosome acts as a substantial barrier to RNAPII progression.

Strikingly, nucleosomes containing either H3K56ac or H3K122ac showed a pronounced increase in run-off transcript production by RNAPII (Figure 1D, lanes 4, 6). In contrast, H3K64ac had little or no effect on the transcription efficiency, which was comparable to the unmodified control (Figure 1D, lane 5). These results demonstrate that specific acetylations within the histone fold domain distinctly modulate the transcription efficiency of RNAPII through the nucleosome.

A quantitative analysis revealed that H3K56ac and H3K122ac increased the fractions of full-length transcripts by approximately three-and five-fold relative to unmodified nucleosomes, respectively (Figure 1E). These effects are comparable to the enhanced nucleosome transcription observed with the H3 N-terminal acetylations, including H3K4ac, H3K9ac, H3K14ac, H3K18ac, H3K23ac, and H3K27ac (Figure 1D, lane 7, and E). Consistent with a previous study (25), the H3 N-terminal acetylations drastically reduce RNAPII pausing at the SHL(-5) position, thereby increasing the pausing population at the SHL(-1) and SHL(0) positions (Figure 1F-H). In contrast, the RNAPII pausing at the SHL(-5) and SHL(-1) positions was not substantially altered in the H3K56ac and H3K122ac nucleosomes (Figure 1F and G). Notably, the RNAPII pausing at the SHL(0) position was significantly alleviated in the H3K56ac and H3K122ac nucleosomes (Figure 1F). Such alleviation of RNAPII pausing at the SHL(0) position was not observed in the nucleosome containing the H3 N-terminal acetylations (Figure 1D, lane 7, and H). Therefore, the acetylation within the histone fold domain may regulate RNAPII transcription differently from the acetylations on the H3 N-terminal tail.

Cryo-EM structures reveal local weakening of histone-DNA contacts by H3K56ac and H3K122ac, but not H3K64ac

To understand the structural basis for the distinct transcriptional outcomes, we determined the cryo-EM structures of the H3K56ac, H3K64ac, and H3K122ac nucleosomes and the unmodified nucleosome used for the nucleosome transcription assays at 2.96, 2.99, 3.07, and 3.07 Å resolutions, respectively (Figure 2A, Table 1, and Supplementary Figure 3-6). We avoided sample crosslinking, which stabilizes histone-DNA contacts in the nucleosome. Instead, we employed a single-chain variable fragment (scFv), PL2-6, which specifically binds to the acidic patch of nucleosomes and effectively isolates the nucleosome sample from the air-water interface, thereby stabilizing the cryo-EM specimen (26).

In the H3K56ac nucleosome, parts of the Lys56 and acetylated Lys56 side chains are resolved, with the visible density appearing to extend toward the SHL(±6) region (Figure 3A). In addition, the density corresponding to the DNA entry/exit region appeared substantially weaker than that of the unmodified nucleosome, suggesting the increased flexibility of the nucleosomal DNA ends (Figure 2A). Since lysine acetylation diminishes its positive charge and thereby weakens the local histone-DNA interactions, the flexibility of the nucleosomal DNA ends may be enhanced by the H3 Lys56 acetylation, which weakens the histone-DNA interactions near the SHL(±6) position despite the overall preservation of the side-chain orientation. Consistently, the DNA ends of the H3K56ac nucleosome were markedly more susceptible to micrococcal nuclease than those of the unmodified nucleosome (Figure 2B-D, Supplementary Figure 7). These results are consistent with previous fluorescence resonance energy transfer studies (19, 27–29). Notably, the leading

Sample	#1 Structure of the unmodified nucleosome (EMD-66767) (PDB ID: 9XDM)	#2 Structure of the H3K56ac nucleosome (EMD-66768) (PDB ID: 9XDN)	#3 Structure of the H3K64ac nucleosome (EMD-66769) (PDB ID: 9XDO)	#4 Structure of the H3K122ac nucleosome (EMD-66770) (PDB ID: 9XDP)
Data collection				
Electron microscope	KriosG4	KriosG4	KriosG4	KriosG4
Camera	K3	K3	K3	K3
Pixel size (Å/pix)	1.06	1.06	1.06	1.06
Defocus range (μm)	-1.25 to -2.25	-1.25 to -2.25	-1.25 to -2.25	-1.25 to -2.25
Exposure time (second)	4.5	4.5	4.5	4.5
Total dose ($e^-/Å^2$)	61.9	60.9	60.6	61.4
Movie frames (no.)	40	40	40	40
Total micrographs (no.)	6 580	8 180	8 071	7 431
Reconstruction				
Software	Relion 5.0	Relion 5.0	Relion 5.0	Relion 5.0
Particles for 2D classification	2 832 919	4 165 413	2 752 619	4 247 723
Particles for 3D classification	684 801	811 976	561 678	669 653
Particles in the final map (no.)	91 479	122 391	124 333	127 356
Symmetry	C1	C1	C1	C1
Final resolution (Å)	3.07	2.96	2.99	3.07
FSC threshold	0.143	0.143	0.143	0.143
Map sharpening B factor ($Å^2$)	-71.248	-71.827	-83.214	-82.055
Model building				
Software	Coot	Coot	Coot	Coot
Refinement				
Software	Phenix, ISOLDE	Phenix, ISOLDE	Phenix, ISOLDE	Phenix, ISOLDE
Model composition				
Protein	726	726	726	721
Nucleotide	268	262	266	264
Validation				
MolProbity score	1.28	0.96	1.28	1.27
Clash score	5.23	1.93	5.25	5.03
R.m.s. deviations				
Bond lengths (Å)	0.004	0.005	0.004	0.004
Bond angles (°)	0.759	0.674	0.761	0.784
Ramachandran plot				
Favored (%)	98.31	98.16	98.30	98.28
Allowed (%)	1.55	1.84	1.56	1.57
Outliers (%)	0.14	0.00	0.14	0.14

Table 1. **Cryo-EM data collection, processing, refinement, and validation statistics**

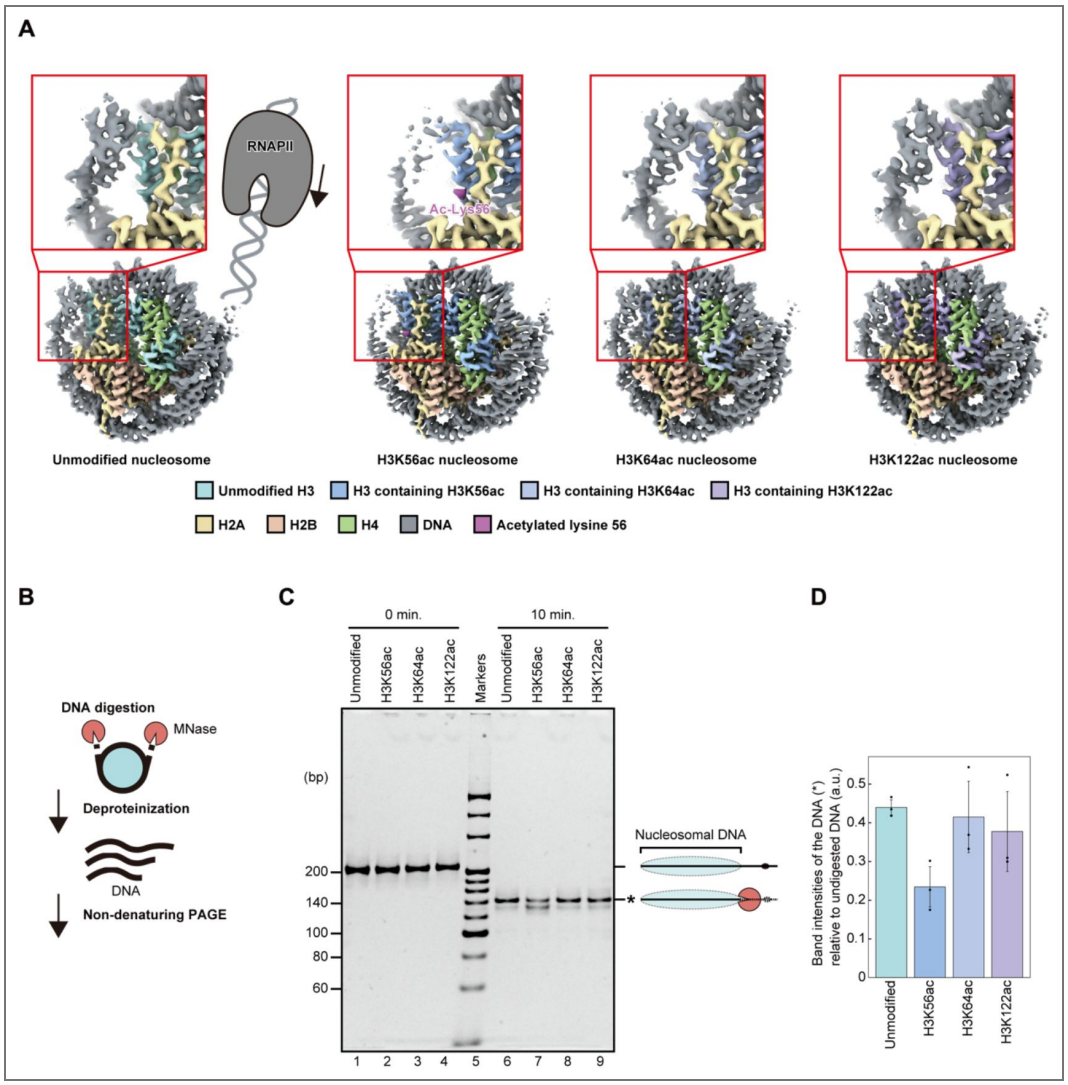

Figure 2. Cryo-EM analysis of the H3K56ac nucleosome reveals weakened density at the entry/exit DNA region.

(A) Cryo-EM density maps of the unmodified, H3K56ac, H3K64ac, and H3K122ac nucleosomes. H2A, H2B, H4, and DNA are colored yellow, red, green, and gray, respectively. H3 in the unmodified, H3K56ac, H3K64ac, and H3K122ac nucleosomes is colored cyan, blue, dark blue, and purple, respectively. The density map corresponding to Ac-Lys56 is shown in magenta. (B) Schematic representation of the micrococcal nuclease digestion assay. (C) Micrococcal nuclease digestion assays of the unmodified, H3K56ac, H3K64ac, and H3K122ac nucleosomes. Deproteinized DNA was analyzed by non-denaturing PAGE and stained with ethidium bromide. (D) Quantification of the micrococcal nuclease assay. Band intensities indicated by asterisks in (C) were normalized with those of the undigested DNA. Bar graphs show the means of three independent experiments, and dots indicate the individual values. Error bars represent the standard deviation.

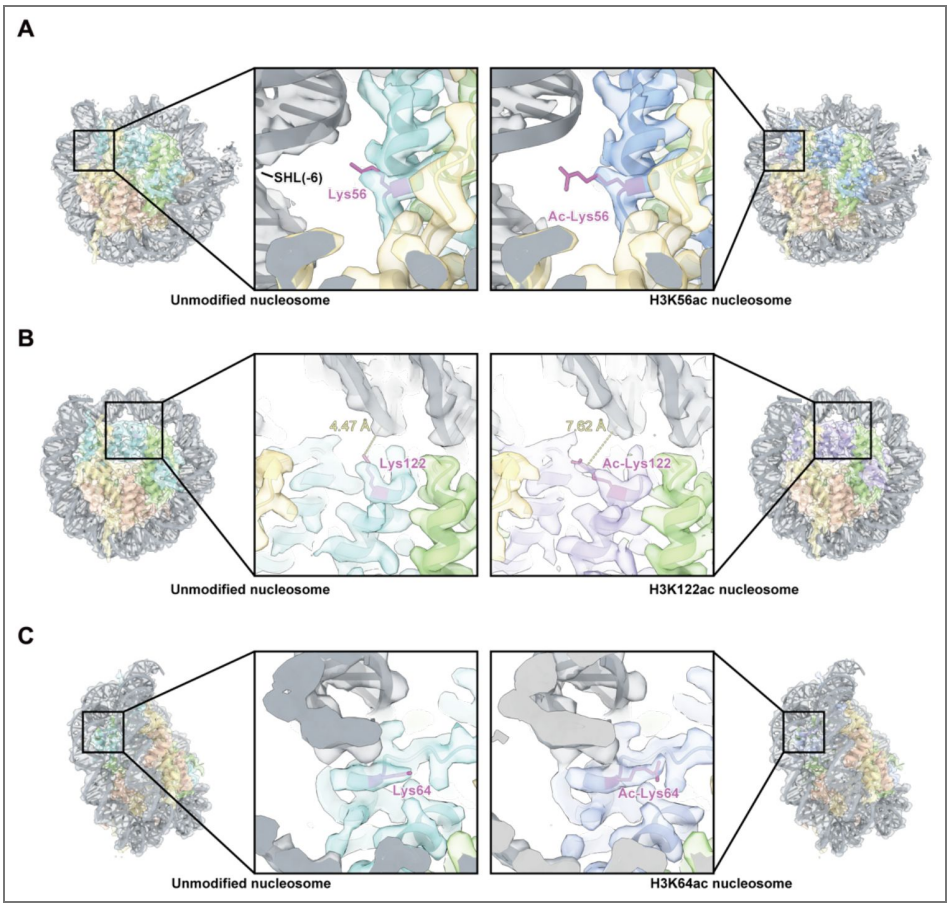

Figure 3. Acetylation at Lys122 of H3 reorients the side chain away from the nucleosomal DNA.

(A-C) Close-up views of the regions surrounding the acetylated residues in H3K56ac (A), H3K122ac (B), and H3K64ac (C) nucleosomes. H2A, H2B, H4, and DNA are colored yellow, red, green, and gray, respectively. H3 in the unmodified, H3K56ac, H3K64ac, and H3K122ac nucleosomes is colored cyan, blue, dark blue, and purple, respectively. Acetylated lysine residues and their corresponding unmodified lysine residues are shown in magenta. The distances between the nitrogen atom at the zeta position of the lysine or acetyl-lysine residue and the nearest oxygen atom of the DNA backbone are shown in (B).

edge of RNAPII sterically clashes with the distal DNA end of the nucleosome upon reaching the SHL(0) position, inducing RNAPII pausing (30). Therefore, the increased flexibility at the distal nucleosomal DNA end may alleviate the RNAPII pausing at the SHL(0) position (Figure 4).

The H3 Lys122 residue directly interacts with the DNA backbone in the unmodified nucleosome. The acetyl group neutralizes the positive charge of the lysine sidechain, thereby diminishing the electrostatic attraction between the histone and DNA, which likely facilitates the partial unwrapping of the nucleosomal DNA near the SHL(0) position. In fact, the acetylation of the H3 Lys122 residue reorients the sidechain away from the nucleosomal DNA (Figure 3B). This may be a major reason why the H3 Lys122 acetylation enhances RNAPII transcription, by alleviating its SHL(0) pausing (Figure 4).

In contrast, the H3K64ac nucleosome displayed nearly identical density and local resolution profiles to the unmodified nucleosome, indicating that this modification does not significantly alter the histone-DNA contacts within the nucleosome core particle (Figure 3C).

Discussion

Our results reveal that the acetylation of lysine within the histone fold domain of H3 has distinct and site-specific effects on RNAPII transcription through nucleosomes. Among the three tested sites, H3K56ac and H3K122ac markedly enhanced transcription, whereas H3K64ac had little influence. Structural analyses by cryo-EM demonstrated that H3K56ac and H3K122ac locally weaken the histone-DNA interactions at the DNA entry/exit region and near the dyad, respectively, providing a direct structural basis for their transcriptional effects. These findings establish a mechanistic link between the site-specific acetylation within the histone fold domain and the regulation of RNAPII transcription by histone acetylation.

The acetylations of the H3 Lys56 and H3 Lys122 residues likely promote transcription by distinct but complementary mechanisms (Figure 4). H3K56ac increases the flexibility of nucleosomal DNA ends, which may lower the energetic barrier for DNA unwrapping and alleviate the RNAPII pausing at the SHL(0) position by reducing steric clashes between RNAPII and the distal nucleosomal DNA end. In contrast, H3K122ac destabilizes the histone-DNA contacts around the dyad, directly weakening the central anchor point of the nucleosome and facilitating the passage of RNAPII through this region. Both effects converge to lower the nucleosomal barrier and enhance transcriptional output, consistent with the observed increases in full-length transcripts. Notably, these mechanisms differ from those mediated by H3 N-terminal acetylations, which mainly affect RNAPII pausing at upstream positions such as SHL(-5) (25). Thus, the acetylation within the histone fold domain modulates transcription through a structural mechanism distinct from that of histone tail acetylations. Previous biochemical studies have suggested that H3K56ac and H3K122ac contribute to chromatin remodeling, histone exchange, and transcriptional activation (18, 20, 21, 31, 32). Our structural data now provide direct evidence that these modifications alter the physical properties of the nucleosome to promote transcriptional elongation.

Although H3K64ac is enriched at transcriptionally active sites, our results indicate that acetylation of H3 Lys64 has minimal impact on RNAPII transcription through nucleosomes or on nucleosome structure. These findings suggest that H3K64ac alone does not directly modulate RNAPII transcription efficiency. Previous studies have reported that H3K64ac promotes histone eviction, raising the possibility that additional factors, such as histone chaperones, are required to facilitate transcription (13). Moreover, H3K64ac is known to co-localize with transcriptionally active histone marks, including H3K27ac, H3K4me1, and H3K122ac, suggesting that H3K64ac may regulate transcription through crosstalk with other PTMs (13, 23). In our H3K64ac nucleosome structure, acetylated Lys64 is shielded by the surrounding DNA, implying that this modification is inaccessible to reader proteins in an intact nucleosome. Therefore, recognition of H3K64ac likely requires nucleosome disruption. Crosstalk between H3K64ac and other PTMs may occur prior to chromatin assembly or during nucleosome-disruptive events.

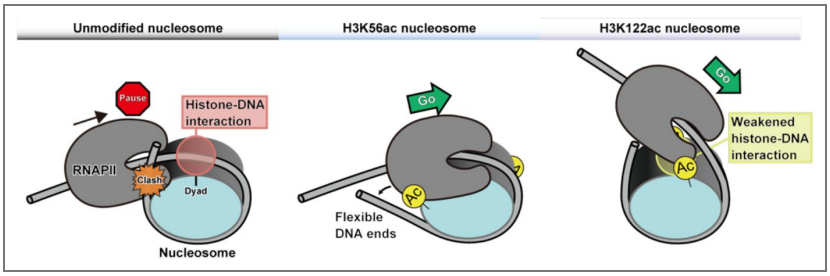

Figure 4. Acetylation at Lys56 and Lys122 of H3 likely promotes transcription through distinct yet complementary mechanisms.

The direct contacts between the distal DNA end of the nucleosome and RNAPII, as well as the histone-DNA interactions near the dyad axis, likely contribute to RNAPII pausing at the SHL(0) position. The acetylation at Lys56 of H3 enhances the flexibility of the DNA ends of the nucleosome, which may alleviate steric clashes between the DNA and RNAPII and facilitate RNAPII passage. In contrast, the acetylation at Lys122 of H3 weakens histone-DNA interactions near the dyad axis, thereby reducing RNAPII pausing and enhancing transcription at the SHL(0) region.

More broadly, our findings highlight the functional diversity of histone acetylation beyond the N-terminal tails. Whereas the N-terminal tail acetylations predominantly recruit effector proteins through bromodomains and other reader modules, histone fold domain acetylations act directly on nucleosomal DNA dynamics(6, 8, 33). This dual mode of regulation, via effector-mediated signaling and direct modulation of nucleosome architecture, may enable cells to precisely coordinate chromatin remodeling and transcription in response to specific cues(34). Our work provides a foundation for future studies to investigate how distinct histone fold domain acetylations interact with other chromatin modifications, remodeling factors, and transcription machinery across different physiological and developmental contexts, thereby advancing our understanding of how the nucleosome structure encodes regulatory information.

Material and methods

Preparation of histones

Human histones H2A, H2B, and H4 were expressed and purified as described previously(35). Briefly, H2A, H2B, and H4 were expressed in Escherichia coli cells. After denaturation of the insoluble fractions, the 6×histidine-tagged histones were purified by Ni-NTA agarose chromatography (Qiagen). The 6×histidine-tags were removed by thrombin protease treatment and the histones were further purified by MonoS cation-exchange chromatography.

Unmodified human histone H3.2 C110A was purified as previously described(36). In summary, the chemically synthesized H3 N-terminal peptide (residues 1-28) was ligated to the recombinant C-terminal regions of H3 (A29C-135, C110A) using the one-pot native chemical ligation method. After desulfurization, the H3 peptide was purified by high performance liquid chromatography. Because cysteine at position 29 was converted to alanine during desulfurization, the resulting peptide contained only the C110A mutation.

The human histone H3.2 C110A acetylated at Lys 56 (H3K56Ac) was previously synthesized(37) and used in this study. The other acetylated histones (H3K64Ac and H3K122Ac) were newly synthesized using a similar procedure. Briefly, the full-length H3.2 sequence was divided into N-terminal, internal, and C-terminal peptide segments. Each segment was prepared through Fmoc solid-phase peptide synthesis as an N-terminal free amine and a C-terminal thioester for the N-terminal segment, an N-terminal thiazolidine (Thz) and a C-terminal thioester for the internal segment, and an N-terminal Cys and a C-terminal carboxylic acid for the C-terminal segment. To assemble the peptide segments, sequential peptide ligation in the C-to-N direction was conducted according to the following procedure: 1) ligation between the internal and C-terminal segments and subsequent Thz-to-Cys conversion in a one-pot manner followed by HPLC purification and 2) ligation between the N-terminal and internal/C-terminal segments followed by HPLC purification. After desulfurization, full-length H3K64Ac and H3K122Ac were isolated as white powders after the final HPLC purification and lyophilization steps.

Preparation of DNA fragment

The 198 bp DNA fragment containing the 9-base mismatched region was purified as previously described(24). In brief, the plasmid containing the modified Widom 601 DNA fragment was amplified in *E. coli*. The Widom 601 DNA fragment was excised from the plasmid DNA by *Eco*RV (Takara), and purified by polyethylene glycol precipitation. After dephosphorylation with alkaline phosphatase (Takara), the DNA fragment was digested with *Bgl*I (Takara). The resulting fragment was purified by a Prep Cell apparatus (Bio-Rad). The purified 153 bp DNA fragment was ligated with the 45 bp DNA fragment containing the 9-base mismatched region by T4 DNA ligase (NIPPON GENE), and further purified by a Prep Cell apparatus (Bio-Rad).

Reconstitution of nucleosomes

The nucleosomes were reconstituted as previously reported(35). In brief, the histone octamers were assembled from H2A, H2B, H4, and either unmodified or acetylated H3 histones, and purified by size-exclusion chromatography on a HiLoad 16/60 Superdex 200 column (Cytiva). The resulting

octamers were mixed with the 198 bp DNA fragment, and the nucleosomes were reconstituted using the salt-dialysis method. The nucleosomes were further purified by a Prep Cell apparatus (Bio-Rad).

Preparation of RNAPII and TFIIS

Komagataella phaffi RNAPII was purified as previously described(38–40). In summary, endogenous Rpb2 containing the tandem affinity purification (TAP) tag was purified from K. phaffi cells by FLAG-affinity column chromatography and anion-exchange column chromatography.

K. phaffi TFIIS was prepared as previously described(40). Briefly, the TFIIS protein was bacterially produced and purified by Ni-affinity column chromatography. After removing the His-tag by HRV-3C protease, the TFIIS protein was further purified by cation-exchange column chromatography.

Transcription assay

The transcription assay was conducted as previously described(24, 25). In brief, the nucleosome and RNAPII were incubated at 30°C for 30 minutes in reaction buffer, containing 0.1 μM nucleosome, 0.1 μM RNAPII, 0.1 μM TFIIS, 26 mM HEPES-KOH (pH 7.5), 50 mM potassium acetate, 0.2 μM zinc acetate, 20 μM Tris(2-carboxyethyl) phosphine, 1.5% glycerol, 0.1 mM dithiothreitol, 5 mM magnesium chloride, 400 μM each ATP, UTP, GTP, and CTP, and 0.4 μM fluorescently labeled RNA primer (5'-DY647-AUAAUUAGCUC-3') (Dharmacon). The reaction was quenched by mixing 2 μl of the reaction mixture and 1 μl of deproteinization solution containing 200 mM Tris-HCl (pH 8.0), 80 mM EDTA, and 0.6 mg/ml proteinase K (Roche), followed by an incubation at room temperature for 10 minutes. Then, 12 μl of Hi-Di formamide was added, and the sample was heated at 95°C for 5 minutes. The sample was analyzed by 10% denaturing PAGE. The DY647 fluorescence of RNA products was detected by an Amersham Typhoon imager (Cytiva). The band intensities of the transcripts were quantified with the ImageQuant™ TL software (GE Healthcare) and normalized with the transcripts of the unmodified nucleosome template.

Purification of PL2-6 scFv

PL2-6 scFv containing (GGGS)4 linker peptides between the heavy and light chains was purified as previously described(25, 26, 41). In short, the scFv was bacterially produced and recovered as an insoluble fraction. After denaturation, the histidine-tagged scFv was purified by Ni-NTA agarose chromatography (Qiagen). The resulting scFv was refolded by dialysis with buffer exchange using a peristaltic pump, and further purified on a HiLoad 26/600 Superdex 75 pg column (Cytiva). Eluted fractions were analyzed by SDS-PAGE under both reducing conditions with an incubation at 95°C for 5 minutes and non-reducing conditions without heating. The binding activity of the scFv in each fraction was assessed by an electrophoretic mobility shift assay using nucleosomes. Fractions exhibiting nucleosome-binding activity were combined, concentrated, and stored at -80°C.

Sample preparation for cryo-EM analysis

Samples of unmodified H3, H3K56ac, H3K64ac, and H3K122ac nucleosomes for cryo-EM analysis were prepared as previously described(25). Nucleosomes (0.5 μM) and 1.5 μM of PL2-6 scFv were mixed in reaction buffer, containing 10 mM HEPES-KOH (pH 7.5), 0.5 mM dithiothreitol, 2.5% glycerol, 10 mM Tris-HCl (pH 7.5), 30 mM sodium chloride, and 0.2 mM EDTA. After an incubation at 30°C for 30 minutes, the mixture was applied to a Quantifoil R1.2/1.3 copper grid and plunge-frozen using a Vitrobot Mark IV (Thermo Fisher Scientific). Grids were glow discharged for 1 minute using a PIB-10 Bombarder (Vacuum Device Inc.) prior to sample application.

Cryo-EM data collection

The cryo-EM data were acquired using the EPU automation software on a Krios G4 electron microscope (Thermo Fisher Scientific). The microscope was operated at 300 kV, with a nominal magnification of 81,000× (corresponding to a pixel size of 1.06 Å), and a defocus range of -1.25 to

-2.25 µm. Micrographs were recorded on a K3 BioQuantum direct electron detector (Gatan) with a 20 eV energy-filter, with a total of 40 frames per movie. The detailed cryo-EM data recording conditions are provided in Table 1.

Image processing

The overall workflow is shown in Supplementary Figure 3-6. The acquired movies were aligned and dose-weighted using MOTIONCOR2(42). CTFFIND4(43) was used to estimate the contrast transfer function (CTF). Relion 5.0(44) was used for image processing. Particles were picked by Laplacian-of-Gaussian based auto picking and subjected to two-dimensional classification, de novo initial model generation, three-dimensional (3D) classification, 3D auto-refinement, Bayesian polishing, and CTF refinement. Junk particles were removed during the classification steps. To focus on the nucleosome structure, 3D classification with a nucleosome mask was conducted with and without alignment. The resolution of the final maps was estimated from the gold standard Fourier shell correlation (FSC = 0.143) criterion. The final cryo-EM map of the H3K56ac nucleosome was flipped along the z-axis using ChimeraX(45).

Model building and refinement

The initial atomic models were built based on the coordinates of the modified Widom 601 DNA sequence from the RNAPII-nucleosome complex (Protein Data Bank (PDB) ID: 6A5O(24)) and the coordinates of the histone octamer from the human nucleosome (PDB ID: 7VZ4(46)). Acetyl-lysine residues were introduced using Coot(47). The atomic coordinates were fitted to the cryo-EM maps by rigid-body fitting using UCSF ChimeraX(45). The fitted coordinates were refined by phenix.real_space_refine(48), and manually adjusted by Coot(47) and ISOLDE(49). Refinement and validation statistics are summarized in Table 1. The distances between atoms were measured using USCF ChimeraX(45).

Micrococcal nuclease assay

Nucleosomes (0.125 µM) were incubated in a reaction mixture, containing 10 mM HEPES-KOH (pH 7.5), 2.5% glycerol, 1.9 mM dithiothreitol, 40 mM Tris-HCl (pH 8.0), 25 mM sodium chloride, 2.5 mM calcium chloride, and 10 mU/µl micrococcal nuclease (Takara) at 37°C for 10 minutes. A 4 µl portion of the reaction mixture was mixed with 2 µl of deproteinization solution, containing 20 mM Tris-HCl (pH 8.0), 20 mM EDTA, 0.1% SDS, and 0.5 mg/ml proteinase K (Roche), and incubated at room temperature for 10 minutes. The samples were analyzed by 8% non-denaturing PAGE and stained with ethidium bromide. Gel images were acquired by an Amersham Imager 680 (Cytiva). The band intensities of the DNA were quantified using the ImageQuant™ TL software (GE Healthcare) and normalized with those of the undigested DNA.

The use of Large Language Models

ChatGPT, a Large Language Model developed by OpenAI, was used in a strictly auxiliary role to support the writing process and graph generation. This included assistance with phrasing, grammar correction, and the generation of code examples in Python. The authors remain fully responsible for the content and conclusions of the manuscript.

Data availability

The cryo-EM maps of the unmodified, H3K56ac, H3K64ac, and H3K122ac nucleosomes were deposited to the Electron Microscopy Data Bank (EMDB) and the Protein Data Bank (PDB), respectively. The accession codes are as follows: unmodified nucleosome (EMD-66767 and PDB ID 9XDM), H3K56ac nucleosome (EMD-66768 and PDB ID 9XDN), H3K64ac nucleosome (EMD-66769 and PDB ID 9XDO), and H3K122ac nucleosome (EMD-66770 and PDB ID 9XDP).

Acknowledgements

We thank Y. Takeda and M. Dacher (The University of Tokyo) for their assistance. We also thank M. Goto and M. Henmi (RIKEN) for their assistance with protein purification.

Additional information

Author contributions

Conceptualization: TO, TK, GH, YT, SSe, HK

Methodology: TO, SH, TK, SSu, KN, GH, SSe, YT, HK

Resources: TO, SSu, KN, GH, JK, YK, HE, HK

Investigation: TO, SH, SSu, KN, GH, YT, HK

Visualization: TO, SH, MO, YT, HK

Funding acquisition: TO, SH, TK, GH, SSe, YT, HK

Project administration: TK, GH, SSe, YT, HK

Supervision: TK, GH, SSe, YT, HK

Writing – original draft: TO, HK

Writing – review & editing: TO, SH, TK, GH, HE, SSe, YT, HK

Funding

Funder	Grant reference number	Author
MEXT | Japan Society for the Promotion of Science (JSPS)	JP25KJ1033	Takumi Oishi
MEXT | Japan Society for the Promotion of Science (JSPS)	JP25K18410	Suguru Hatazawa
MEXT | Japan Society for the Promotion of Science (JSPS)	JP23K17392	Tomoya Kujirai
MEXT | Japan Society for the Promotion of Science (JSPS)	JP24H00062	Shun-ichi Sekine Tomoya Kujirai
MEXT | Japan Society for the Promotion of Science (JSPS)	JP25K24594	Hitoshi Kurumizaka
MEXT | Japan Society for the Promotion of Science (JSPS)	JP24H02319	Hitoshi Kurumizaka
MEXT | Japan Society for the Promotion of Science (JSPS)	JP24H02328	Hitoshi Kurumizaka
MEXT | Japan Science and Technology Agency (JST)	JPMJSP2108	Takumi Oishi
MEXT | Japan Science and Technology Agency (JST)	JPMJPR25N9	Tomoya Kujirai
MEXT | Japan Science and Technology Agency (JST)	https://doi.org/10.52926/jpmjer1901	Hitoshi Kurumizaka
MEXT | Japan Science and Technology Agency (JST)	https://doi.org/10.52926/jpmjcr24t3	Hitoshi Kurumizaka
Japan Agency for Medical Research and Development (AMED)	JP25ama121002	Yoshimasa Takizawa
Japan Agency for Medical Research and Development (AMED)	JP25ama121009	Hitoshi Kurumizaka Gosuke Hayashi

Author ORCID iDs

Hitoshi Kurumizaka: https://orcid.org/0000-0001-7412-3722

Additional files

Supplementary figures

References

1. **Luger K,** Dechassa ML, Tremethick DJ (2012) New insights into nucleosome and chromatin structure: an ordered state or a disordered affair?. *Nat Rev Mol Cell Biol* **13**:436-447 https://doi.org/10.1038/nrm3382 | PubMed
2. **Luger K,** Mäder AW, Richmond RK, Sargent DF, Richmond TJ (1997) Crystal structure of the nucleosome core particle at 2.8 Å resolution. *Nature* **389**:251-260 https://doi.org/10.1038/38444 | PubMed
3. **McGinty RK,** Tan S (2015) Nucleosome structure and function. *Chem Rev* **115**:2255-2273 https://doi.org/10.1021/cr500373h | PubMed
4. **Koyama M,** Kurumizaka H (2018) Structural diversity of the nucleosome. *J Biochem* **163**:85-95 https://doi.org/10.1093/jb/mvx081 | PubMed
5. **Wolffe AP,** Hayes JJ (1999) Chromatin disruption and modification. *Nucleic Acids Res* **27**:711-720 https://doi.org/10.1093/nar/27.3.711 | PubMed
6. **Cosgrove MS,** Boeke JD, Wolberger C (2004) Regulated nucleosome mobility and the histone code. *Nat Struct Mol Biol* **11**:1037-1043 https://doi.org/10.1038/nsmb851 | PubMed
7. **Bowman GD,** Poirier MG (2015) Post-translational modifications of histones that influence nucleosome dynamics. *Chem Rev* **115**:2274-2295 https://doi.org/10.1021/cr500350x | PubMed
8. **Strahl BD,** Allis CD (2000) The language of covalent histone modifications. *Nature* **403**:41-45 https://doi.org/10.1038/47412 | PubMed
9. **Eberharter A,** Becker PB (2002) Histone acetylation: a switch between repressive and permissive chromatin. *EMBO Rep* **3**:224-229 https://doi.org/10.1093/embo-reports/kvf053 | PubMed
10. **Zhao Z,** Shilatifard A (2019) Epigenetic modifications of histones in cancer. *Genome Biol* **20**:1-16 https://doi.org/10.1186/s13059-019-1870-5 | PubMed
11. **Tropberger P,** Schneider R (2010) Going global: Novel histone modifications in the globular domain of H3. *Epigenetics* **5**:112-117 https://doi.org/10.4161/epi.5.2.11075 | PubMed
12. **Iwasaki W,** Tachiwana H, Kawaguchi K, Shibata T, Kagawa W, Kurumizaka H (2011) Comprehensive structural analysis of mutant nucleosomes containing lysine to glutamine (KQ) substitutions in the H3 and H4 histone-fold domains. *Biochemistry* **50**:7822-7832 https://doi.org/10.1021/bi201021h | PubMed
13. **Di Cerbo V,** Mohn F, Ryan DP, Montellier E, Kacem S, Tropberger P, et al. (2014) Acetylation of histone H3 at lysine 64 regulates nucleosome dynamics and facilitates transcription. *eLife* **3**:e01632 https://doi.org/10.7554/eLife.01632 | PubMed
14. **Williams SK,** Truong D, Tyler JK (2008) Acetylation in the globular core of histone H3 on lysine-56 promotes chromatin disassembly during transcriptional activation. *Proc Natl Acad Sci U S A* **105**:9000-9005 https://doi.org/10.1073/pnas.0800057105 | PubMed
15. **Li Q,** Zhou H, Wurtele H, Davies B, Horazdovsky B, Verreault A, et al. (2008) Acetylation of histone H3 lysine 56 regulates replication-coupled nucleosome assembly. *Cell* **134**:244-255 https://doi.org/10.1016/j.cell.2008.06.018 | PubMed
16. **Downs JA** (2008) Histone H3 K56 acetylation, chromatin assembly, and the DNA damage checkpoint. *DNA Repair* **7**:2020-2024 https://doi.org/10.1016/j.dnarep.2008.08.016 | PubMed
17. **Das SK,** Huynh MT, Lee TH (2023) Spontaneous histone exchange between nucleosomes. *J Biol Chem* **299**:105037 https://doi.org/10.1016/j.jbc.2023.105037 | PubMed

18. **Manohar M,** Mooney AM, North JA, Nakkula RJ, Picking JW, Edon A, et al. (2009) Acetylation of histone H3 at the nucleosome dyad alters DNA-histone binding. *J Biol Chem* **284**:23312-23321 https://doi.org/10.1074/jbc.m109.003202 | PubMed

19. **Simon M,** North JA, Shimko JC, Forties RA, Ferdinand MB, Manohar M, et al. (2011) Histone fold modifications control nucleosome unwrapping and disassembly. *Proc Natl Acad Sci U S A* **108**:12711-12716 https://doi.org/10.1073/pnas.1106264108 | PubMed

20. **Tropberger P,** Pott S, Keller C, Kamieniarz-Gdula K, Caron M, Richter F, et al. (2013) Regulation of transcription through acetylation of H3K122 on the lateral surface of the histone octamer. *Cell* **152**:859-872 https://doi.org/10.1016/j.cell.2013.01.032 | PubMed

21. **Chatterjee N,** North JA, Dechassa ML, Manohar M, Prasad R, Luger K, et al. (2015) Histone acetylation near the nucleosome dyad axis enhances nucleosome disassembly by RSC and SWI/SNF. *Mol Cell Biol* **35**:4083-4092 https://doi.org/10.1128/mcb.00441-15 | PubMed

22. **Suzuki Y,** Horikoshi N, Kato D, Kurumizaka H (2016) Crystal structure of the nucleosome containing histone H3 with crotonylated lysine 122. *Biochem Biophys Res Commun* **469**:483-489 https://doi.org/10.1016/j.bbrc.2015.12.041 | PubMed

23. **Pradeepa MM,** Grimes GR, Kumar Y, Olley G, Taylor GCA, Schneider R, et al. (2016) Histone H3 globular domain acetylation identifies a new class of enhancers. *Nat Genet* **48**:681-686 https://doi.org/10.1038/ng.3550 | PubMed

24. **Kujirai T,** Ehara H, Fujino Y, Shirouzu M, Sekine S, Kurumizaka H (2018) Structural basis of the nucleosome transition during RNA polymerase II passage. *Science* **362**:595-598 https://doi.org/10.1126/science.aau9904 | PubMed

25. **Oishi T,** Hatazawa S, Kujirai T, Kato J, Kobayashi Y, Ogasawara M, et al. (2023) Contributions of histone tail clipping and acetylation in nucleosome transcription by RNA polymerase II. *Nucleic Acids Res* **51**:10364-10374 https://doi.org/10.1093/nar/gkad754 | PubMed

26. **Zhou BR,** Yadav KNS, Borgnia M, Hong J, Cao B, Olins AL, et al. (2019) Atomic resolution cryo-EM structure of a native-like CENP-A nucleosome aided by an antibody fragment. *Nat Commun* **10**:2301 https://doi.org/10.1038/s41467-019-10247-4 | PubMed

27. **Neumann H,** Hancock SM, Buning R, Routh A, Chapman L, Somers J, et al. (2009) A method for genetically installing site-specific acetylation in recombinant histones defines the effects of H3 K56 acetylation. *Mol Cell* **36**:153-163 https://doi.org/10.1016/j.molcel.2009.07.027 | PubMed

28. **Shimko JC,** North JA, Bruns AN, Poirier MG, Ottesen JJ (2011) Preparation of fully synthetic histone H3 reveals that acetyl-lysine 56 facilitates protein binding within nucleosomes. *J Mol Biol* **408**:187-204 https://doi.org/10.1016/j.jmb.2011.01.003 | PubMed

29. **North JA,** Shimko JC, Javaid S, Mooney AM, Shoffner MA, Rose SD, et al. (2012) Regulation of the nucleosome unwrapping rate controls DNA accessibility. *Nucleic Acids Res* **40**:10215-10227 https://doi.org/10.1093/nar/gks747 | PubMed

30. **Ehara H,** Kujirai T, Shirouzu M, Kurumizaka H, Sekine S (2022) Structural basis of nucleosome disassembly and reassembly by RNAPII elongation complex with FACT. *Science* **377**:eabp9466 https://doi.org/10.1126/science.abp9466 | PubMed

31. **Topal S,** Vasseur P, Radman-Livaja M, Peterson CL (2019) Distinct transcriptional roles for histone H3-K56 acetylation during the cell cycle in yeast. *Nat Commun* **10**:4372 https://doi.org/10.1038/s41467-019-12400-5 | PubMed

32. **Hyun K,** Ahn J, Kim H, Kim J, Kim YI, Park HS, et al. (2024) The BAF complex enhances transcription through interaction with H3K56ac in the histone globular domain. *Nat Commun* **15**:9614 https://doi.org/10.1038/s41467-024-53981-0 | PubMed

33. **Musselman CA,** Lalonde ME, Côté J, Kutateladze TG (2012) Perceiving the epigenetic landscape through histone readers. *Nat Struct Mol Biol* **19**:1218-1227 https://doi.org/10.1038/nsmb.2436 | PubMed

34. **Xie W,** Song C, Young NL, Sperling AS, Xu F, Sridharan R, et al. (2009) Histone H3 lysine 56 acetylation is linked to the core transcriptional network in human embryonic stem cells. *Mol Cell* **33**:417-427 https://doi.org/10.1016/j.molcel.2009.02.004 | PubMed

35. **Kujirai T,** Arimura Y, Fujita R, Horikoshi N, Machida S, Kurumizaka H (2018) Methods for preparing nucleosomes containing histone variants. In: Orsi GA, Almouzni G (Eds). *Histone Variants: Methods and Protocols* **1832** New York, NY: Springer New York. pp. 3-20 https://doi.org/10.1007/978-1-4939-8663-7_1 | PubMed

36. **Hao F,** Murphy KJ, Kujirai T, Kamo N, Kato J, Koyama M, et al. (2020) Acetylation-modulated communication between the H3 N-terminal tail domain and the intrinsically disordered H1 C-terminal domain. *Nucleic Acids Res* **48**:11510-11520 https://doi.org/10.1093/nar/gkaa949 | PubMed

37. **Nakatsu K,** Yanase M, Hayashi G, Okamoto A (2020) Fmoc-compatible and C-terminal-sequence-independent peptide alkyl thioester formation using cysteinylprolyl imide. *Org Lett* **22**:4670-4674 https://doi.org/10.1021/acs.orglett.0c01450 | PubMed

38. **Higo T,** Suka N, Ehara H, Wakamori M, Sato S, Maeda H, et al. (2014) Development of a hexahistidine-3× FLAG-tandem affinity purification method for endogenous protein complexes in Pichia pastoris. *J Struct Funct Genomics* **15**:191-199 https://doi.org/10.1007/s10969-014-9190-1 | PubMed

39. **Ehara H,** Umehara T, Sekine S, Yokoyama S (2017) Crystal structure of RNA polymerase II from Komagataella pastoris. *Biochem Biophys Res Commun* **487**:230-235 https://doi.org/10.1016/j.bbrc.2017.04.039 | PubMed

40. **Ehara H,** Yokoyama T, Shigematsu H, Yokoyama S, Shirouzu M, Sekine SI (2017) Structure of the complete elongation complex of RNA polymerase II with basal factors. *Science* **357**:921-924 https://doi.org/10.1126/science.aan8552 | PubMed

41. **Zhou BR,** Bai Y (2021) Preparation of scFv stabilized chromatosomes for single-particle cryo-EM structure determination. *STAR Protoc* **2**:100396 https://doi.org/10.1016/j.xpro.2021.100396 | PubMed

42. **Zheng SQ,** Palovcak E, Armache JP, Verba KA, Cheng Y, Agard DA (2017) MotionCor2: Anisotropic correction of beam-induced motion for improved cryo-electron microscopy. *Nat Methods* **14**:331-332 https://doi.org/10.1038/nmeth.4193 | PubMed

43. **Rohou A,** Grigorieff N (2015) CTFFIND4: Fast and accurate defocus estimation from electron micrographs. *J Struct Biol* **192**:216-221 https://doi.org/10.1016/j.jsb.2015.08.008 | PubMed

44. **Scheres SHW** (2012) RELION: Implementation of a Bayesian approach to cryo-EM structure determination. *J Struct Biol* **180**:519-530 https://doi.org/10.1016/j.jsb.2012.09.006 | PubMed

45. **Goddard TD,** Huang CC, Meng EC, Pettersen EF, Couch GS, Morris JH, et al. (2018) UCSF ChimeraX: Meeting modern challenges in visualization and analysis. *Protein Sci* **27**:14-25 https://doi.org/10.1002/pro.3235 | PubMed

46. **Takizawa Y,** Ho C.-H, Sato S, Danev R, Kurumizaka H (2025) High-resolution cryo-EM analyses of nucleosomes. In: Gaudreau L, Guillemette B (Eds). *Histones: Methods and Protocols* **2919** New York, NY: Springer New York. pp. 91-107

47. **Emsley P,** Lohkamp B, Scott WG, Cowtan K (2010) Features and development of Coot. *Acta Crystallogr Sect D Biol Crystallogr* **66**:486-501 https://doi.org/10.1107/s0907444910007493 | PubMed

48. **Liebschner D,** Afonine PV, Baker ML, Bunkoczi G, Chen VB, Croll TI, et al. (2019) Macromolecular structure determination using X-rays, neutrons and electrons: recent developments in Phenix. *Acta Crystallogr Sect D Struct Biol* **75**:861-877 https://doi.org/10.1107/s2059798319011471 | PubMed

49. **Croll TI** (2018) ISOLDE: A physically realistic environment for model building into low-resolution electron-density maps. *Acta Crystallogr Sect D Struct Biol* **74**:519-530 https://doi.org/10.1107/s2059798318002425 | PubMed

Peer reviews

Reviewer #1 (Public review):

Summary:

The authors investigate how site-specific acetylation within the histone H3 folded domain affects RNA polymerase II transcription through nucleosomes. They focus on H3K56ac, H3K64ac, and H3K122ac, prepare chemically defined nucleosomes carrying each modification, and compare their effects using an in vitro transcription assay, cryo-electron microscopy structures, and micrococcal nuclease sensitivity assays.

The main finding is that H3K56ac and H3K122ac increase production of full-length run-off transcripts and reduce pausing near the nucleosomal dyad region, whereas H3K64ac has little detectable effect under the same reconstituted conditions. The structural analyses suggest that H3K56ac weakens or destabilizes DNA near the entry/exit region, while H3K122ac alters histone-DNA contacts near the dyad. These observations support a model in which different acetylation sites within the H3 folded domain influence nucleosomal transcription barriers through distinct local effects on histone-DNA interactions.

This is a useful study because it examines histone core-domain acetylation using chemically defined nucleosomes and directly compares several modifications in the same experimental system. However, the broader cellular context of these modifications is not sufficiently developed, and some mechanistic conclusions rely on correlations between static nucleosome structures and endpoint transcription assays rather than direct observation of polymerase passage through modified nucleosomes.

Strengths:

(1) The study uses site-specifically acetylated H3 proteins and reconstituted nucleosomes, allowing direct comparison of H3K56ac, H3K64ac, and H3K122ac under controlled conditions.

(2) The combination of transcription assays, cryo-electron microscopy, and nuclease sensitivity assays provides multiple lines of evidence, particularly for increased DNA end flexibility in H3K56ac nucleosomes.

(3) The authors analyze unmodified, H3K56ac, H3K64ac, and H3K122ac nucleosomes in parallel, with reported structural resolutions of approximately 3 Angstroms and accompanying validation materials.

(4) The negative result for H3K64ac is informative, because it distinguishes the direct effect of this modification in a minimal reconstituted system from prior cellular associations with active chromatin and histone eviction.

The comparison with H3 N-terminal acetylation highlights that acetylation within the folded domain may affect transcription at different positions or by different mechanisms than tail acetylation.

Weaknesses:

The rationale for focusing on H3K56ac, H3K64ac, and H3K122ac has not been developed sufficiently. The manuscript would benefit from a clearer summary of what is known about the abundance of these modifications in cells, the enzymes or histone metabolic pathways that may introduce or remove them, and whether they are thought to occur before histone deposition, on assembled nucleosomes, or during nucleosome remodeling.

The central mechanistic model is based mainly on correlations between structures of free nucleosomes and endpoint transcription assays. The study does not directly observe RNA polymerase II paused at or passing through the relevant nucleosomal positions, so the proposed link between local structural changes and reduced pausing should be stated with appropriate caution.

The H3K56ac interpretation is supported by both structural observations and nuclease sensitivity data, but the map comparison underlying the reduced entry/exit DNA density is still mostly qualitative. The manuscript should more clearly state the map comparison conditions, such as contouring and local map quality, so that non-specialist readers can judge how robust the local density differences are.

The H3K122ac mechanism is plausible, but the evidence for dyad destabilization is more indirect. The main support comes from the orientation of the K122 side chain and its distance from DNA, while an independent biochemical test of dyad-region destabilization is not provided.

The transcription assay appears to include statistical testing, but the figure legend and methods should more clearly state which tests were used, what comparisons were made, how n was defined, and whether multiple-comparison correction was applied.

The relationship between the 198 bp transcription template, the linker DNA, the 9-base mismatched region, and the DNA regions modeled in the cryo-electron microscopy structures is somewhat difficult to follow. This does not necessarily require new experiments, but a clearer explanation would help readers connect the transcription assay design with the structural models.

The use of H3.2 C110A for chemical ligation and the use of the PL2-6 single-chain antibody fragment for cryo-electron microscopy sample stabilization are reasonable technical choices, but their purposes and possible effects on interpretation should be explained more clearly for readers outside structural biology.

Because the work uses a minimal in vitro system with human nucleosomes and Komagataella phaffii RNA polymerase II/TFIIS, the conclusions should be limited to direct physical effects on nucleosome transcription barriers unless cellular cofactors, remodelers, histone chaperones, additional modifications, and nucleosome positioning are addressed or discussed.

https://doi.org/10.7554/eLife.111802.1.sa2

Reviewer #2 (Public review):

Summary:

Chromatin regulates a wide range of biological processes. The nucleosome, composed of 147 bp of DNA wrapped around a histone octamer containing histones H2A, H2B, H3, and H4, is the fundamental unit of chromatin. Post-translational modifications of histone proteins regulate the dynamic properties of nucleosomes and thereby influence chromatin accessibility and gene expression. Among these modifications, lysine acetylation on histone H3 is closely associated with transcriptional activation. While the epigenetic functions of acetylation on the histone H3 N-terminal tail have been extensively studied, the molecular mechanisms by which acetylation within the histone H3 core domain, particularly at Lys56, Lys64, and Lys122, modulates nucleosome architecture to facilitate RNA polymerase II (RNAPII) transcription remain unclear.

In this study, Oishi et al. investigated the effects of histone H3 acetylation at K56, K64, and K122 on RNAPII transcription using in vitro transcription assays. Furthermore, the authors

determined the three-dimensional structures of nucleosomes containing these acetylation marks by cryo-electron microscopy single-particle analysis, revealing distinct structural dynamics depending on the acetylation site. Overall, this study advances our understanding of the molecular mechanisms linking histone H3 core acetylation to transcriptional regulation.

Strengths:

(1) Site-specifically acetylated histone H3 proteins were chemically synthesized using a unique and rational peptide ligation strategy, representing a major technical strength of this study.

(2) The in vitro transcription assays demonstrated that H3K56ac and H3K122ac increase the production of run-off transcripts, whereas H3K64ac has little effect on transcription efficiency. These findings highlight the distinct functional roles of individual acetylation sites within the histone H3 core domain.

(3) The cryo-EM structures of nucleosomes containing either H3K56ac or H3K122ac revealed that H3 acetylation weakens histone-DNA interactions, providing a structural basis for the observed effects on transcription.

Weaknesses:

(1) Although the biochemical and structural data are convincing and sufficiently support the authors' conclusions, complementary cellular experiments would further strengthen the physiological relevance of the in vitro findings. While such experiments are not essential for supporting the main claims of the study, they would enhance the overall impact and biological significance of the work.

(2) Although the authors demonstrate the structural consequences of individual H3 core acetylation events, the study does not investigate potential synergistic effects among multiple acetylated lysine residues within the H3 core domain. Consequently, the relationship between combinatorial acetylation patterns and their collective impact on RNA polymerase II-mediated transcription remains unclear.

https://doi.org/10.7554/eLife.111802.1.sa1

Reviewer #3 (Public review):

This is a short and punchy manuscript that nicely summarises the 4 structures that are determined and provides a basis for the differences seen for acetylation sites shown for RNAPII activity.

The authors build on previous biochemical work that determined the functional outcomes of H3 core acetylation, adapting an assay they have previously used extensively to investigate RNAPII transcription on nucleosomes and, indeed, even H3 N-terminal tail acetylation. This assay is as such well set up and has a wealth of confirmatory previous studies from this lab and the authors are careful not to overanalyse their results, leading to robust and well-considered results. The structures are determined to a high resolution, allowing the interpretation put forward about side chain orientations, with clear densities shown for the regions of interest.

Further discussion or experiments would strengthen the conclusions further:

(1) The conclusion on the role of H3K56Acetylation could be strengthened, especially as the results are somewhat counterintuitive. It is conceptually surprising that acetylation near the entry/exit DNA that destabilises this region also leads to a reduced stall propensity at the

dyad but has a limited effect at SHL5? While it can be explained by the clash at the dyad pause being reduced, the more direct effect of DNA breathing amplification would be expected to have a larger effect at SHL 5. Indeed, the density for DNA at SHL5 appears to be weaker in Figure 2A, suggesting the entry/exit DNA flexibility is amplified past this region.

Perhaps another assay that looks more directly at the flexibility of the entry/exit DNA would be useful, either through restriction enzyme-mediated cleavage or FRET (DNA ends and H2AK119 labels), providing stronger evidence of this effect. MNase is rather indirect and similar to the RNAPII assay itself.

Similarly, were the authors surprised by the modest effect (less than 2-fold) in transcriptional pause at SHL 0 for the K122Ac? Presumably, based on the model in Figure 4, this would be expected to be the area with the largest effect? The results of K56Ac and K122Ac almost seem swapped to what would be expected in Figure 1H. Further discussion of this observation would be useful.

(2) Could the local weakening of DNA, especially at the dyad, be observed in the cryo-EM structures? Perhaps comparison of local resolution estimation differences in this region compared to unmodified would be useful.

(3) Caution should be taken, and discussion should include that the structural data presented is after extensive processing. Many nucleosome averaging classes were discarded in the 3D classification steps (nicely summarised in Table 1 as "particles for 3d classification" and "particles in final map"). Indeed, it is likely that higher DNA flexibility particles would be thrown away during this processing step. This can be observed for K56Ac DNA ordering, for example, in Supplementary Figure S4, yellow and cyan classes from the round of 3D classification look to be high resolution and have a higher order of DNA, so there has been some selection here. How was this done? While this is not fully quantifiable, it gives an idea of the extent of wrapping. We would suggest discussing the methodological limitations and showing the models after the first auto refinement to see if the features discussed on end flexibility and dan ordering are retained.

(4) Di Cerbo et al. (reference 13) showed acetylation at K64 alters salt stability and affects transcription. Why do the authors think there is a discrepancy, albeit with different assays? Direct reference and discussion of this in the text should be included.

(5) Why was H3.2 used, while this is relatively abundant in mouse cells, human protein was used, and this appears to be less common than H3.1 and H3.3. We are sure that the effect is not likely to be substantive on structure (as shown by the Kurumizaka lab previously), but should be addressed in the text

https://doi.org/10.7554/eLife.111802.1.sa0